Structural Engineering and Mechanics, *Vol. 69, No. 4 (2019) 467-477*
DOI: https://doi.org/10.12989/sem.2019.69.4.467

Tensile and fracture characterization using a simplified digital image correlation test set-up

Abhishek Kumar*[1,2], S. Vishnuvardhan[1,2a], A. Ramachandra Murthy[1b] and G. Raghava[1c]

[1]*CSIR – Structural Engineering Research Centre, Chennai, India*
[2]*Academy of Scientific and Innovative Research (AcSIR), India*

(Received November 14, 2018, Revised December 31, 2018, Accepted January 10, 2019)

Abstract. Digital image correlation (DIC) is now a popular and extensively used full-field metrology technique. In general, DIC is performed by using a turnkey solution offered by various manufacturers of DIC. In this paper, a simple and economical set-up for DIC is proposed which uses easily accessible digital single-lens reflex (DSLR) camera rather than industrial couple-charged device (CCD) cameras. The paper gives a description of aspects of carrying a DIC experiment which includes experimental set-up, specimen preparation, image acquisition and analysis. The details provided here will be helpful to carry DIC experiments without specialized DIC testing rig. To validate the responses obtained from proposed DIC set-up, tension and fatigue tests on specimens made of IS 2062 Gr. E300 steel are determined. Tensile parameters for a flat specimen and stress intensity factor for an eccentrically-loaded single edge notch tension specimen are evaluated from results of DIC experiment. Results obtained from proposed DIC experiments are compared with those obtained from conventional methods and are found to be in close agreement. It is also noted that the high resolution of DSLR allows the use of proposed approach for fracture characterization which could not be carried out with a typical turnkey DIC solution employing a camera of 2MP resolution.

Keywords: digital image correlation; DSLR; fracture characterization; SIF; tensile properties

1. Introduction

The use of theoretical models and numerical methods in design and structural integrity assessment of mechanical components sometimes is restricted by the complications in finding material and fracture parameters from experimental data. Full-field measurement technique is a metrology technique, which allows estimation of displacement, strain or stress over surface of the tested specimen or component. In present times, use of advanced materials and complex structures demands full-field non-contact measurement and investigation techniques. Traditionally, pointwise strain gauge technique measurement has been used in such scenario. This method is tedious, requires elaborate instrumentation and is not very suitable for either field or real time application. Optical method is a very popular and widely used alternative as they are non-intrusive, non-contact and non-destructive (Rastogi 2000, Dournaux *et al.* 2009). All full-field non-contact optical metrologies are broadly classified into interferometric techniques and non-interferometric techniques as shown in Fig. 1 (Pan *et al.* 2009).

Interferometric metrologies use difference in phase of scattered light waves from test object surface before and after deformation. Because of the working principle, these techniques require a coherent light source. The results are in the form of fringe patterns, to obtain the field variables (displacements, strains or stresses) from fringe pattern phase analysis and fringe processing have to be carried out. Due to the above-mentioned reasons, measurements are to be taken in a vibration free isolated optical bench in the laboratory. Interferometric techniques cannot be used for real time applications. Non-interferometric techniques determine the surface deformation from difference in grey scale intensity of object surface before and after deformation. Grid methods (Grédiac *et al.* 2016) and digital image correlation (DIC) (Peters and Ranson 1982) are two popular non-interferometric techniques. These techniques work with ordinary white light and surface preparation just involves creation of high contrast speckle. Over a period, the method has grown and been used with other concepts like stereovision, extended finite element methods, X-ray tomography which allows application of DIC to newer problems. It is useful to see DIC as a technique which borrows elements from digital image processing, numerical computing and the domain where it is has to be applied, in present case mainly solid mechanics and fracture mechanics (Fig. 3). With the constant emergence of high spatial-resolution and high-time-resolution image acquisition equipment, the 2D-DIC method can easily be applied to areas where conventional methods could not be applied. It reduces the instrumentation and is not intrusive to make DIC a perfect experimental technique to obtain parameter of constitutive models for biomaterials and composites or dynamic fracture characterization.

*Corresponding author, Scientist
E-mail: abhishek@serc.res.in
[a]Senior Scientist
[b]Principal Scientist
[c]Former Chief Scientist

http://www.techno-press.com/journals/sem&subpage=7
ISSN: 1225-4568 (Print), 1598-6217 (Online)

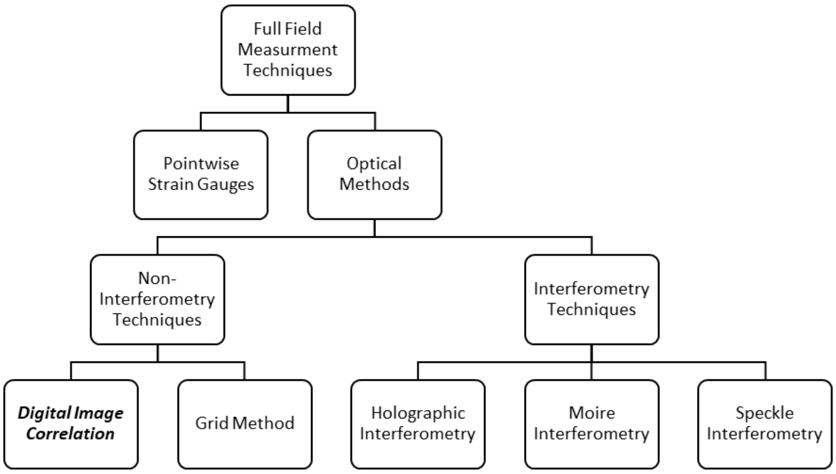

Fig. 1 Classification of full-field measurement techniques

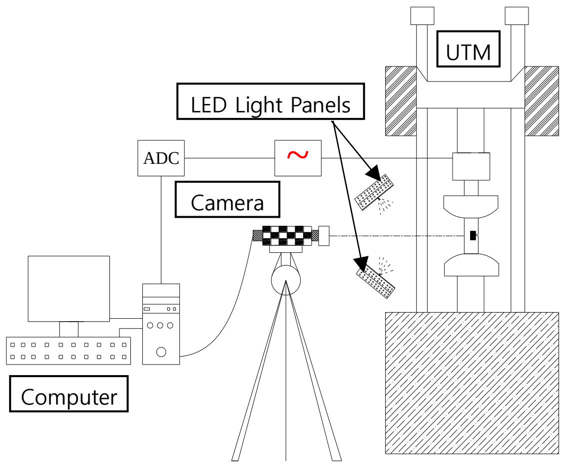

Fig. 2 Typical experimental set-up for a 2D-DIC experiment

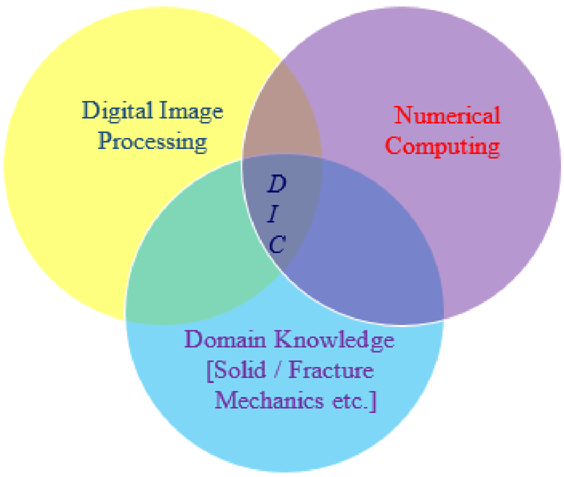

Fig. 3 Digital Image Correlation

Table 1 Variants of digital image correlation technique

Reference	Variants of DIC	Remarks
(Peters and Ranson 1982)	2D-DIC	DIC used for in-plane surface displacement measurement
(Luo *et al.* 1993)	3D-DIC (Stereo-DIC)	Surface three dimensional displacement measurement using concepts of stereovision together with DIC
(Bay *et al.* 1999)	DVC (V-DIC)	Sub surface displacement measurement from X-ray computed tomography images
(Réthoré *et al.* 2007)	X-DIC	Application of XFEM enrichment function in Q4-DIC
(Roux and Hild 2008)	I-DIC	DIC used for identification together with FE simulation
(Tippur and Periasamy 2013)	DGS	Uses angular deflections of light rays propagating through optically transparent solids that are subjected to non-uniform mechanical stress fields
(Hild *et al.* 2016)	T4-DIC	Integration of sensor and imaging data into numerical procedures for the purpose of identification of constitutive relations and their validation.

The early development in DIC was mainly carried out at University of South Carolina (Peters and Ranson 1982). From the inception of DIC in 1982 by Peters and Ranson in University of South Carolina, many variations of DIC have emerged. When concepts of DIC is clubbed with those of binocular stereovision, we have a form of DIC commonly referred to as 3D-DIC or stereo-DIC, which is capable of measuring out-of-plane displacements and strains (Luo *et al.* 1993, Helm and Sutton 1996). In X-ray tomography (Maire and Withers 2014), CCD detectors capable of recording digital images combined with improvements in computer power are used for three dimensional reconstruction of a specimen. When DIC principles are used on these images, we have a variant of DIC, which is known as Volumetric DIC (V-DIC). In some literature it is also referred to as Digital Volume Correlation (DVC) (Bay *et al.* 1999, Regez *et al.* 2008, Buljac *et al.* 2018). DIC has also been used in problems of crack growth where concepts of eXtended Finite Element Method (XFEM) have been applied for development of a new form of DIC popularly known as X-DIC (Julien 2007). Finite element software outputs together with results from DIC have been used for prediction of elastoplastic material (Shang *et al.* 2013) and crack growth parameters and the methodology is termed as I-DIC (Roux and Hild 2008). Very recently, a form of DIC is proposed which uses data from sensor together with finite element analysis and images of the experiment for solving

Table 2 Commonly used correlation criterion

CORRELATION CRITERION	Cross-Correlation (CC)	$C_{CC}=\sum_{i=-N}^{N}\sum_{j=-N}^{N}\left[f(x_i,y_j)\times g(x_i',y_j')\right]$
	Normalized cross-correlation (NCC)	$C_{NCC}=\sum_{i=-N}^{N}\sum_{j=-N}^{N}\left[\frac{f(x_i,y_j)\times g(x_i',y_j')}{\bar{f}\bar{g}}\right]^2$
	Zero-normalized cross-correlation (NCC)	$C_{ZNCC}=\sum_{i=-N}^{N}\sum_{j=-N}^{N}\left[\frac{[f(x_i,y_j)-f_n]\times[g(x_i',y_j')-g_n]}{\Delta f\Delta g}\right]$
SUM-SQUARED DIFFERENCE CORRELATION CRITERION	Sum of squared difference (SSD)	$C_{SSD}=\sum_{i=-N}^{N}\sum_{j=-N}^{N}\left[f(x_i,y_j)-g(x_i',y_j')\right]$
	Normalized sum of squared difference (NSSD)	$C_{NSSD}=\sum_{i=-N}^{N}\sum_{j=-N}^{N}\left[\frac{f(x_i,y_j)}{\bar{f}}-\frac{g(x_i',y_j')}{\bar{g}}\right]^2$
	Zero-normalized sum of squared difference (ZNSSD)	$C_{ZNSSD}=\sum_{i=-N}^{N}\sum_{j=-N}^{N}\left[\frac{f(x_i,y_j)-f_n}{\Delta f}-\frac{g(x_i',y_j')-g_n}{\Delta g}\right]^2$

identification problems, the DIC technique is termed as T4-DIC (Hild *et al.* 2016). Table 1 presents the popular variants of DIC and their application.

Following are few of the salient features of DIC which makes the technique attractive and popular.

- Simple experimental setup
- Easy specimen preparation
- Can be used for any material
- Suitable for in situ measurement
- Can be used for real time experimentation
- Scale independent
- Non-destructive and non-intrusive technique
- Easy adaptability with other imaging techniques
- Can be used together with finite element software
- Provides both accurate numerical data and qualitative visual results

Particle image velocity (PIV) (Westerweel *et al.* 2013), which is extensively used in experimental fluid mechanics for evaluating velocity field in a fluid flow, has a very similar working principle of DIC. In this paper, a brief working of 2D-DIC is discussed. The paper also presents a simple 2-dimensional digital image correlation set-up and procedure, which is used for evaluation of tensile and fracture parameters through DSLR as imaging device.

2. Principles of 2D digital image correlation

The overall goal of DIC is to obtain displacement and strain fields within a region of interest (ROI) for a material sample undergoing deformation. To achieve this goal, implementation of a displacement mapping function, a correlation criterion and a scheme for subpixel interpolation are essential. In DIC experiment images of a sample are taken as it deforms and these images are used as input to a typical DIC program. The idea is to obtain a one-to-one correspondence between material points in the reference (initial undeformed picture) and current (subsequent deformed pictures) configurations. DIC does this by taking small subsections of the reference image, called subsets, and determining their respective locations in the current configuration. The centre of subset is called 'marker'. Once the location of subset in current configuration is located which is carried out by establishing the best correspondence between the square area of the subset in the reference image and the square area in a subsequent image. A correlation criterion is used for establishing best correspondence; list of correlation criterion that are used is shown in Table 2. For each subset, we obtain displacement of the marker information through the transformation used to match the location of the subset in the current configuration. Many subsets are picked in the reference configuration, often with a spacing parameter to reduce computational cost (also note that subsets typically overlap as well). The end result is a grid of points with displacement information with respect to the reference configuration, also referred to as Lagrangian displacements/strains. The displacement/strain fields can then either be reduced or interpolated to form a "continuous" displacement/strain field. In order to allow the deformation of the subset and therefore improving the correlation, different shape functions (mapping functions) may be used. Deformation is assumed to be homogenous and to establish deformation continuity a transformation coordinate in form of Eq. (1) is formed.

$$\begin{aligned} \boldsymbol{x_i'} &= \boldsymbol{x_i} + \boldsymbol{\xi}(\boldsymbol{x_i},\ \boldsymbol{y_i}) \\ \boldsymbol{y_i'} &= \boldsymbol{y_i} + \boldsymbol{\eta}(\boldsymbol{x_i},\ \boldsymbol{y_i}) \end{aligned} \tag{1}$$

In the present work, the reference subset is mapped to the target subset by a second-order mapping function (Lu and Cary 2000) which allows to depict more complicated deformation. The mapping function is given as

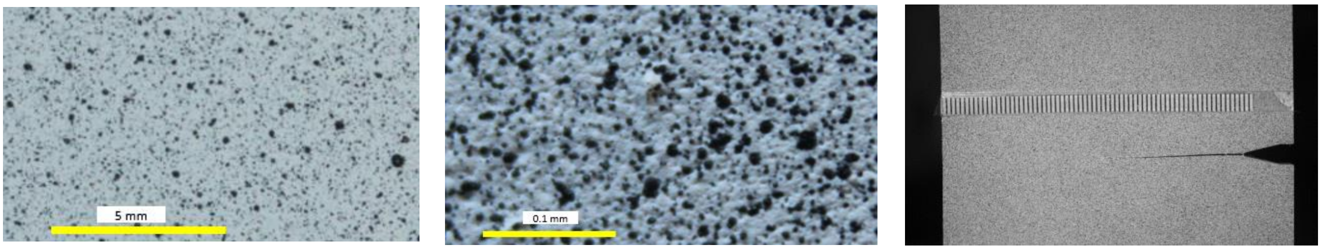

(a) (b) (c)

Fig. 4 Speckle pattern on the specimen

$$
\begin{aligned}
\boldsymbol{x}_i' &= \boldsymbol{x}_i + \boldsymbol{u} + \frac{\partial u}{\partial x}\Delta\boldsymbol{x} + \frac{\partial u}{\partial y}\Delta\boldsymbol{y} + \frac{1}{2}\frac{\partial^2 u}{\partial x^2}\Delta\boldsymbol{x}^2 + \\
&\quad \frac{1}{2}\frac{\partial^2 u}{\partial y^2}\Delta\boldsymbol{y}^2 + \frac{1}{2}\frac{\partial^2 u}{\partial x \partial y}\ \Delta\boldsymbol{x}\ \ \Delta\boldsymbol{y} \\
\boldsymbol{y}_i' &= \boldsymbol{y}_i + \boldsymbol{v} + \frac{\partial v}{\partial x}\Delta\boldsymbol{x} + \frac{\partial v}{\partial y}\Delta\boldsymbol{y} + \frac{1}{2}\frac{\partial^2 v}{\partial x^2}\Delta\boldsymbol{x}^2 + \\
&\quad \frac{1}{2}\frac{\partial^2 v}{\partial y^2}\Delta\boldsymbol{y}^2 + \frac{1}{2}\frac{\partial^2 v}{\partial x \partial y}\ \Delta\boldsymbol{x}\ \ \Delta\boldsymbol{y}
\end{aligned}
\qquad (2)
$$

2.1 Two dimensional digital image correlation set-up

Three steps are to be carried out for computation of displacement and strain fields using 2D-DIC. The three steps are: (i) Specimen preparation, (ii) Image acquisition and (iii) Computation of strains. This section gives the brief description about these steps.

2.1.1 Specimen preparation

Pattern application involves imparting a random texture on the surface of a specimen. The speckle is applied to have contrast in image subsets for better results from correlation algorithm. Specimen is thoroughly cleaned with emery sheet and acetone to remove any dust and moisture on the surface. The specimen is kept under the sun light before laying of speckle pattern. White paint (matte finish) is sprayed on the specimen and the specimen is kept for drying in a dirt free environment for 30 minutes. To get the desired speckle pattern, black paint is sprayed from a distance. The distance of application decides the speckle quality, which is to be determined as per resolution of the image and application. Good speckle pattern is one of the most important aspects of obtaining good and precise results. Lionello and Cristifolini (2014) suggested a thumb rule for a good speckle, that the suggested average size of speckle dots should be three times the size of pixel of the image captured from camera. Fig. 4 presents the obtained speckled pattern on specimen used for evaluation of SIF on an eccentrically-loaded single edge notch tension [ESE(T)] specimen at various magnifications. The specimen is fitted between the grips and the verticality of the specimen is to be checked up with clinometer. It is to be ensured that axis of the camera lens is perpendicular to plane of the specimen by using a calibration grid pattern before start of the test.

In Table 2,

$$f_n = \frac{1}{(2N+1)^2}\sum_{i=-N}^{N}\sum_{j=-N}^{N} f(x_i.y_j),$$

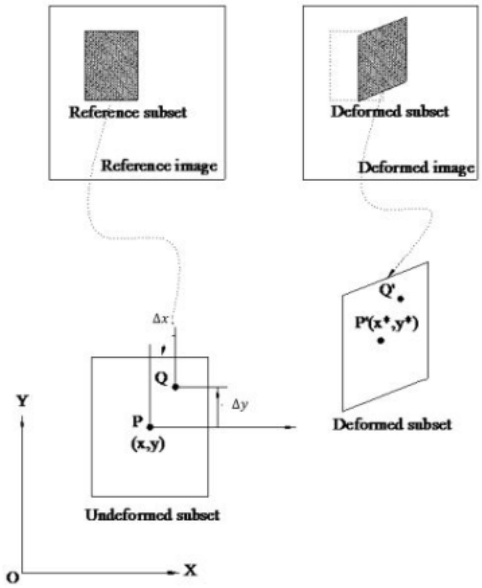

Fig. 5 Schematic illustration of a subset deformation

$$g_n = \frac{1}{(2N+1)^2}\sum_{i=-N}^{N}\sum_{j=-N}^{N} g(x_i'.y_j'),$$

$$\overline{f} = \sqrt{\sum_{i=-N}^{N}\sum_{j=-N}^{N}[f(x_i.y_j)]^2},$$

$$\overline{g} = \sqrt{\sum_{i=-N}^{N}\sum_{j=-N}^{N}[g(x_i'.y_j')]^2},$$

$$\Delta f = \sqrt{\sum_{i=-N}^{N}\sum_{j=-N}^{N}[f(x_i.y_j) - f_m]^2},$$

$$\Delta g = \sqrt{\sum_{i=-N}^{N}\sum_{j=-N}^{N}[g(x_i'.y_j') - g_m]^2}.$$

2.1.2 Image acquisition

As DIC algorithms are applied on images and hence quality of images greatly influences accuracy of displacement values obtained from the experiment. Even the best to be algorithms cannot give accurate displacement values if the image quality is poor. The quality of the

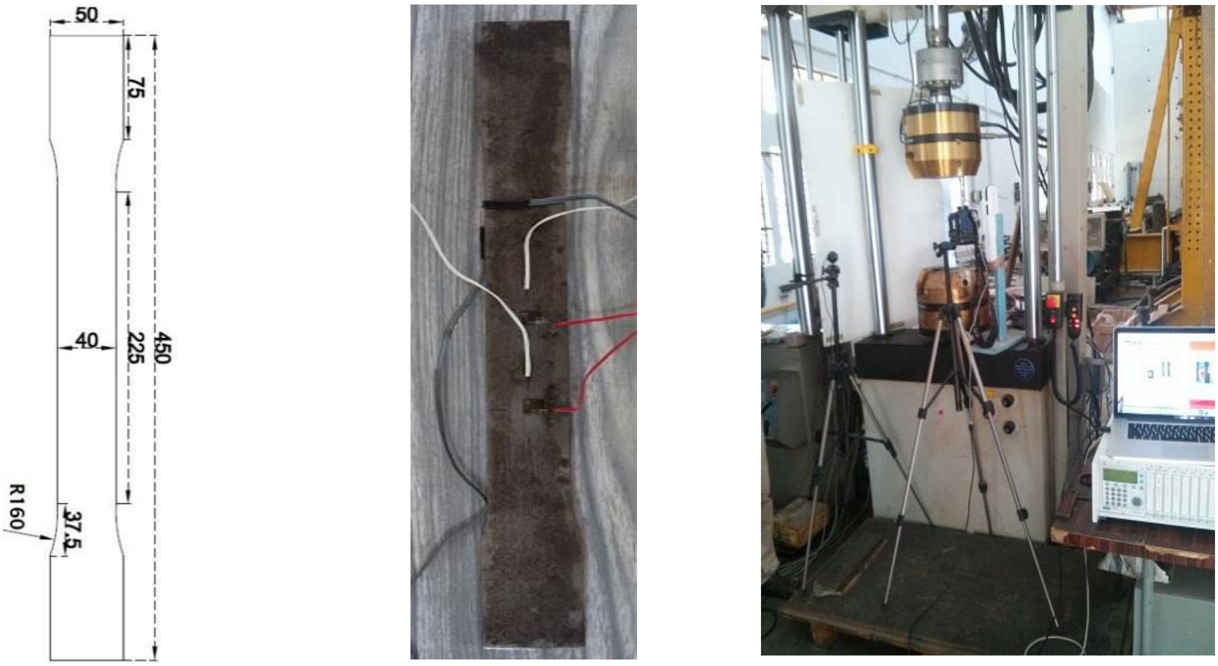

(a) Dimensions (in mm) (b) Instrumentation (c) Test set-up

Fig. 6 Details of tensile test

images depends on camera sensors, lighting and image capture.

(a) Camera sensors**:** Generally, CCD sensors are preferred over CMOS. The resolution and camera setting are important factors that determine final quality of the images. The ISO should be kept to a lowest value as per the lighting.

(b) Lighting: As the working principle of a DIC algorithm is conservation of brightness. So even a slight variation in lighting can result in a wrong displacement values. It is very important to maintain an even lighting for an experiment. A DC powered LED source should be used for a DIC experiment.

(c) Image capture: Any vibration in camera set-up should be avoided, so a trigger is used to capture images. For tests where image capture can be programmed use of programmable trigger is preferred. Camera should be mounted at a stable place preferably on a tripod. It should be made sure that the legs of tripod do not slip under the weight of camera.

Images are taken from a DSLR, Canon 550D with an ISO setting (measure of sensitivity to light) of the camera set to 100 to minimize the noise. To avoid fluctuation in lighting, two DC powered LED light arrays are used. The shutter speed is adjusted to 1/40. To further minimize the vibration, shutter lock feature of the camera is used. In order to get the high quality and unprocessed images, the images are captured in RAW file format (.raw). A python script is written to convert '.raw' images to '.png' images in the same script a luminosity based algorithm is implemented to convert colored image into grey scale.

2.1.3 Computation of strain field

Arriving at displacement field in a DIC technique is multistep process. The strain field is computed from the evaluated full-field displacement. In a general, subset based digital image correlation involves the following activities to arrive at the strain field from a 2D-DIC experiment:

(a) Selection of correlation criterion
(b) Discrete displacement measurement at markers
(c) Selection of calculation path
(d) Selection of basis function or displacement mapping function
(e) Sub-pixel displacement algorithm
(f) Strain field estimation

In subset-based DIC algorithms, the reference image is partitioned into smaller regions referred to as subsets. The deformation is assumed to be homogeneous inside each subset, and the deformed subsets are then tracked in the current image. To evaluate the similarity degree between the reference subset and the deformed subset, a cross-correlation criterion is defined. The matching procedure is completed through searching the peak position of the distribution of correlation coefficient. Once the correlation coefficient extremum is detected, the position of the deformed subset is determined. The differences in the positions of the reference subset center and the target subset center yield the in-plane displacement vector at point P, as illustrated in Fig. 5 which gives a schematic illustration of a reference square subset before deformation and a target (or deformed) subset after deformation. DIC analysis is performed to obtain displacement and strain fields using a MATLAB based open source software, Ncorr v1.2 (Blaber *et al*. 2015).

3. Evaluation of tensile and fracture parameters

(a) (b) (c) (d) (e)

Fig. 7(a) Reference Image with ROI (b) Deformed image at 100 kN (c) Deformed image at 125 kN (d) Deformed image at 157 kN (e) Deformed image at failure load

Knowledge of material and fracture parameter is an important and necessary requirement to carry out analytical, finite element analysis and design. DIC experiment with DSLR as imaging device discussed in the previous sections are used for evaluation of tensile parameter of IS 2062 Gr. E300 steel and for evaluation of stress intensity factor for an ESE(T) specimen made of same material.

3.1 Evaluation of tensile parameters

Tension tests on specimen made of IS 2062 Gr. E300 steel is carried on Instron UTM with ±250 kN capacity. Speckle pattern is applied over specimen surface for generating a surface with high contrast. Fig. 6(a) shows the dimensions of the specimen as per ASTM E8 used for testing (ASTM E8/E8M-16a Standard Test Methods for Tension Testing of Metallic Materials 2016). To get the desired speckle pattern, black paint was applied from a distance of 30 cm from the specimen. Strain and crosshead displacement data is also recorded from strain gauge and UTM. The specimen is attached with two post yield strain gauges placed at the back of the painted surface and two linear strain gauges in the thickness direction as shown in Fig. 6(b). The strain gauges are connected to the data acquisition system. For maintaining the constant white light source, two LED light array having DC power supply is fitted. The entire set-up of the test is shown in Fig. 6(c). The images of size 3456 x 5184 pixels are obtained using the image acquisition system. Since the 2D-DIC system does not give any stress readings, corresponding load for each image should be noted. In order to find the in-plane full field strain measurements from the images captured during experiment, they need to be processed by a correlation algorithm. A forward analysis is used in the present work for evaluation of displacement.

Fig. 7 shows the reference and deformed images for various load levels which are used as input for the correlation algorithm. The region of interest is shown in Fig. 7(a). Paint peel off can be observed in lower part of the specimen in Fig. 7(e) which occurred after the ultimate load is reached. To avoid paint peel off, thickness of paint should be just good enough to get a high contrast speckle. Analysis of captured images are carried out to compute displacements and strains, which are shown in Figs. 8 and 9

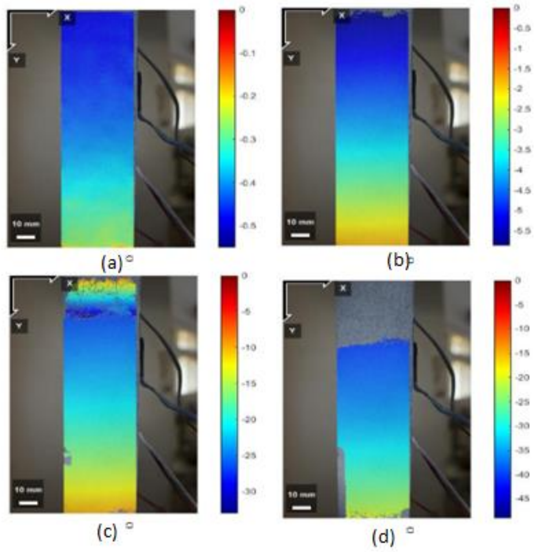

Fig. 8 Displacements (a) at100 kN (b) at 125 kN (c) at 157 kN (d) at failure load

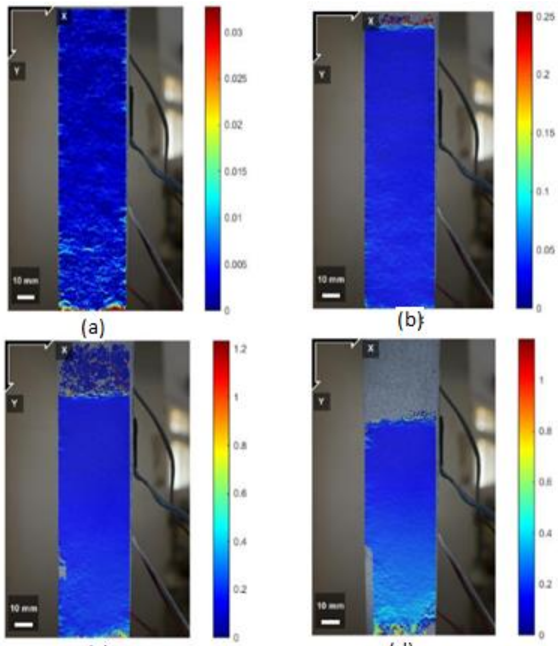

Fig. 9 Strains (a) at 100 kN (b) at 125 kN (c) at 157kN (d) at failure load

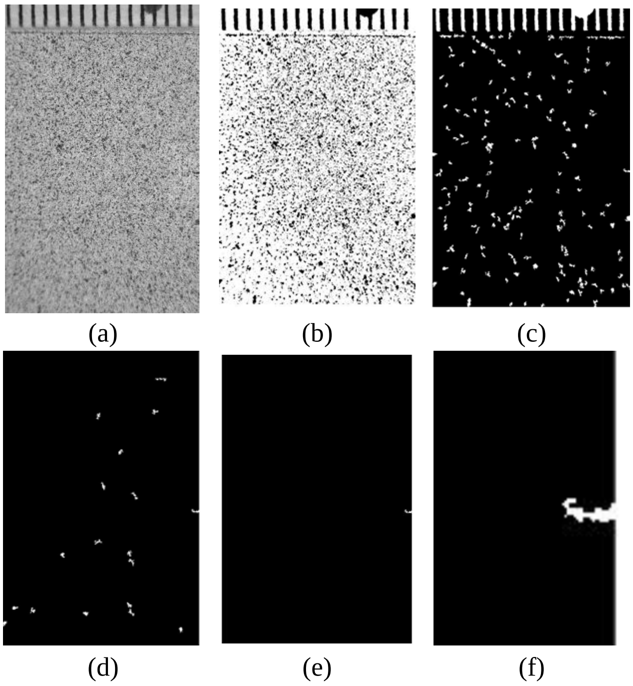

Fig. 10 Image processing to locate crack-tip

respectively.

3.2 Fracture characterization

Digital image correlation gives full-field displacement as output. Stress intensity factor (SIF) is one of the important fracture parameters required for structural integrity evaluation (Ayatollahi and Sedighiani 2010, Jhung and Park 1999). SIF is evaluated from post processing of the displacement field. The evaluation of SIF involves two steps, (1) location of crack-tip and (2) fitting displacement data into stress field equation to evaluate SIF. Yoneyama *et al.* (2007) used DIC for evaluation of mixed-mode SIF using DIC. They used non-linear least squares algorithm for evaluation of SIF and crack-tip is located by minimizing the error in with the theoretically reconstructed displacement field by varying crack-tip location when compared with experimentally obtained displacement values. Harilal *et al.* (2015) presented a least squares approach for evaluation of stress field parameters and the location of crack-tip was assumed to be known. Fatigue crack growth (FCG) studies are carried out on an eccentrically-loaded single edge notch tension (ESE(T)) specimen made of IS 2062 Gr. E 300 steel. ASTM E 647 is followed in preparing the test specimen and carrying out the fatigue experiment (*ASTM E647-15e1 Standard Test Method for Measurement of Fatigue Crack Growth Rates* 2015). Constant amplitude sinusoidal cyclic load is applied using a ±250 kN capacity fatigue rated UTM. The applied load durning FCG tests is decided as per ASTM E1820 (*ASTM E1820-18 Standard Test Method for Measurement of Fracture Toughness* 2018). The maximum and minimum load values are 15 kN and 1.5 kN respectively; the stress ratio is 0.1.

$$\begin{Bmatrix}\sigma_x\\ \sigma_y\\ \tau_{xy}\end{Bmatrix} = \sum_{n=1}^{\infty}\frac{n}{2}A_{In}r^{\frac{n-2}{2}}\begin{pmatrix}\left\{2+(-1)^n+\frac{n}{2}\right\}cos\left(\frac{n}{2}-1\right)\theta-\left(\frac{n}{2}-1\right)cos\left(\frac{n}{2}-3\right)\theta\\ \left\{2-(-1)^n+\frac{n}{2}\right\}cos\left(\frac{n}{2}-1\right)\theta+\left(\frac{n}{2}-1\right)cos\left(\frac{n}{2}-3\right)\theta\\ -\left\{(-1)^n+\frac{n}{2}\right\}sin\left(\frac{n}{2}-1\right)\theta+\left(\frac{n}{2}-1\right)sin\left(\frac{n}{2}-3\right)\theta\end{pmatrix} - \sum_{n=1}^{\infty}\frac{n}{2}A_{IIn}r^{\frac{n-2}{2}}\begin{pmatrix}\left\{2-(-1)^n+\frac{n}{2}\right\}sin\left(\frac{n}{2}-1\right)\theta-\left(\frac{n}{2}-1\right)sin\left(\frac{n}{2}-3\right)\theta\\ \left\{2+(-1)^n-\frac{n}{2}\right\}sin\left(\frac{n}{2}-1\right)\theta+\left(\frac{n}{2}-1\right)sin\left(\frac{n}{2}-3\right)\theta\\ -\left\{(-1)^n-\frac{n}{2}\right\}cos\left(\frac{n}{2}-1\right)\theta-\left(\frac{n}{2}-1\right)cos\left(\frac{n}{2}-3\right)\theta\end{pmatrix} \quad (3)$$

MATLAB code is written to locate the crack-tip using image processing methodology. Simple digital image processing (DIP) algorithms like image inversion, filtering and the fact that crack starts from left side of the image are used. The steps involved in the image-processing program are shown in Fig. 10.

SIF is computed using elastic strain field and stress field equations (Eq. (3)) of Atluri and Kobayashi (Atluri and Kobayashi 1993) for the mixed mode case in general form. Strain field obtained from DIC analysis is shown in Fig. 11(c). To obtain the stress field parameter, a set of over deterministic linear equations are solved using linear least squares method. The value of SIF for Mode I is obtained by using the Eq. (4). The value of stress intensity factor obtained is $47.54 MPa\sqrt{m}$. Fig. 11(c) shows strain field obtained using DIC.

$$\boldsymbol{A_{I1} = K_1/\sqrt{2\pi}} \quad (4)$$

Strain field using expression of Atluri and Kobayashi is plotted and shown in Fig. 12(a) for obtained value of SIF. While taking data for least squares fitting, it is ensured that it does not belong to inelastic region (regions with linear elastic stress more than yield stress) or the far field region which are shown in Fig. 12(b).

4. Results and discussion

Stress-strain curves are obtained from actuator's crosshead displacement values and using DIC results. Fig. 13 shows the comparison of elastic stress-strain data obtained from extensometer and DIC. The slope of the stress-strain data in elastic zone gives the value of Young's modulus. The value of Young's modulus obtained from extensometer and DIC are 209.8 *GPa* and 199.4 *GPa* respectively. Fig. 14 shows the comparison of ratio of lateral strain to longitudinal strain (Poisson's ratio) at three locations on the test specimen obtained from strain gauge readings and DIC results. The value of Poisson's ratio obtained from the DIC results is 0.283 and from strain gauges reading, the value obtained as 0.282. It can be noted that the values obtained from DIC results through a simplified test set-up is in very close agreement with those obtained from strain gauge readings. Fig. 15 shows the comparison of engineering stress-strain curves obtained for rectangular specimen having aspect ratio of 4.91 using extensometer readings and DIC results. The plot shows that the two curves match well up to the ultimate point. After the ultimate stress, the paint used for creating speckle started peeling off and DIC could not be used beyond this point. Fig. 16 shows the comparison of true stress-logarithmic strain curve obtained from extensometer and the true stress-

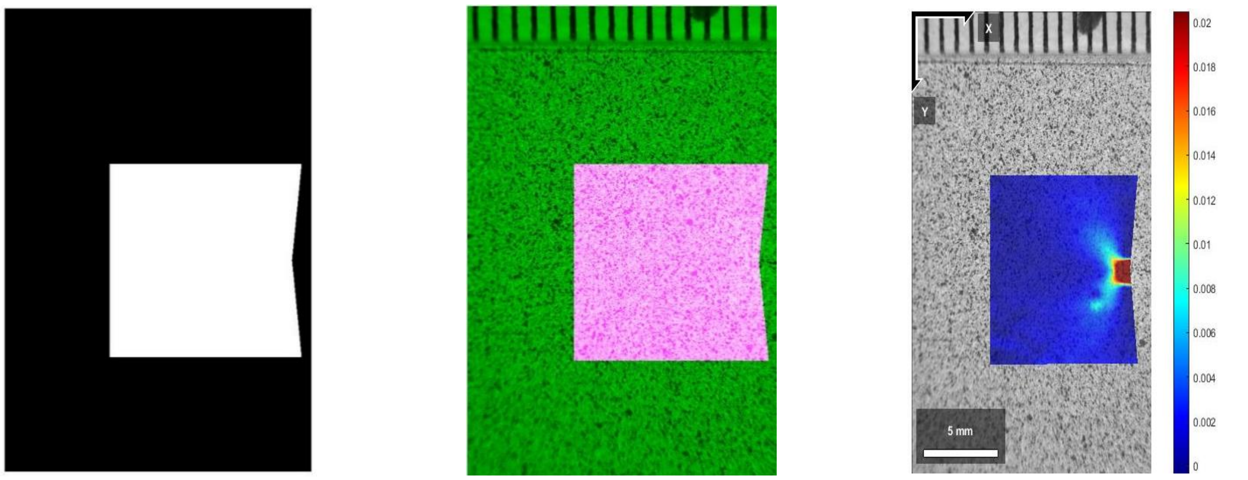

(a) ROI (b) ROI superimposed over the specimen (c) Strain field obtained using DIC

Fig. 11 ROI and strain field obtained from DIC

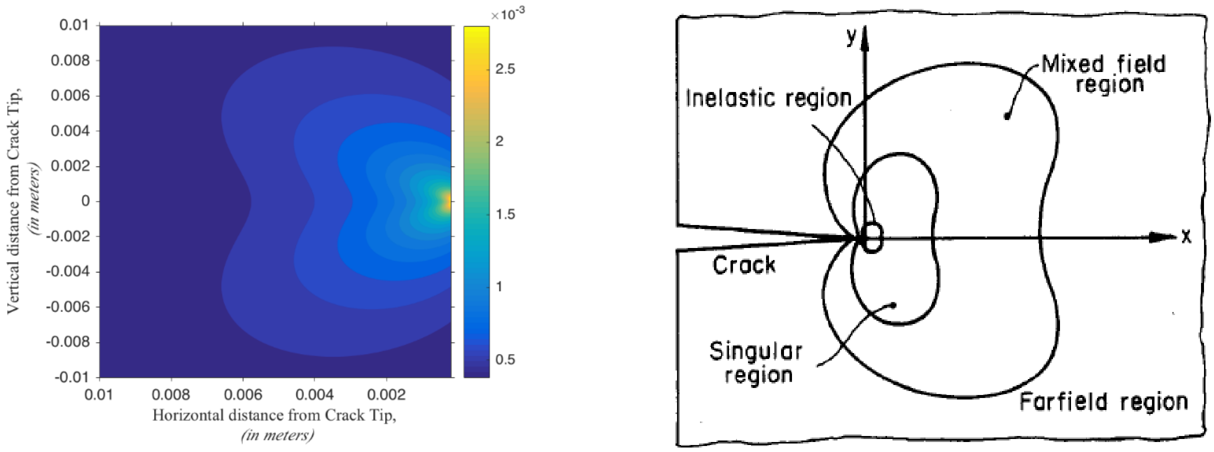

(a) Strain field obtained from the theoretical expression (Atluri and Kobayashi 1993)

(b) Qualitative representation of various zones near crack-tip

Fig. 12 Strain field from expressions of Atluri and Kobayashi and various zones near crack-tip

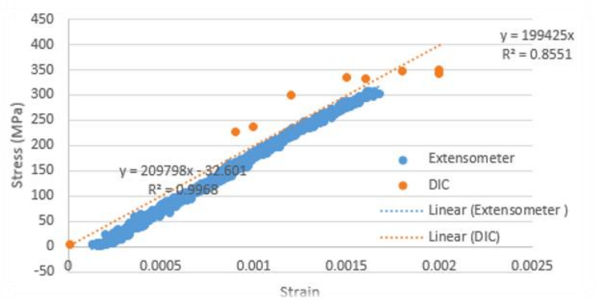

Fig. 13 Comparison of Young's modulus results from extensometer results and DIC results

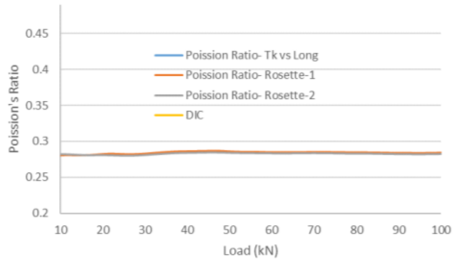

Fig. 14 Comparison of Poisson's ratio values from strain gauge readings and DIC results

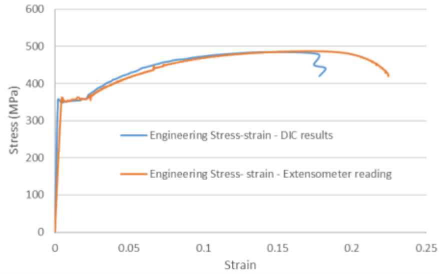

Fig. 15 Comparison of Engineering stress-strain for rectangular specimen using DIC and extensometer reading

full field strain curve obtained from DIC results. The plot shows the slight reduction of stresses after the upper yield, the DIC technique also captured it. Fig. 17 shows the comparison of power law hardening exponent (n) obtained from experimental results and DIC results, the corresponding values are 0.204 and 0.210 respectively.

Table 3 gives the tensile parameters obtained from conventional methods (using strain gauges and extensometer) and DIC results. From Table 3, it can be

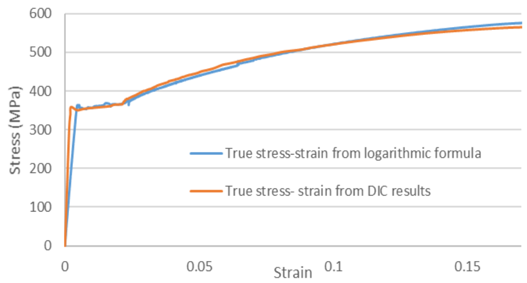

Fig. 16 Comparison of true stress-strain curves obtained for rectangular specimen from extensometer readings and DIC results

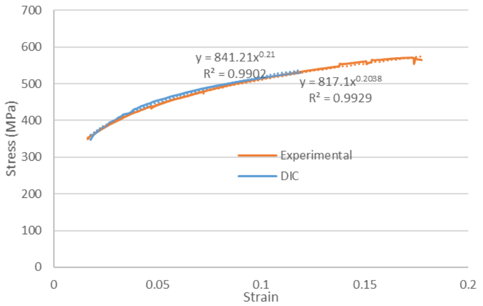

Fig. 17 Comparison of power law hardening exponent (n) from extensometer reading and DIC

Table 3 Tensile parameters obtained from DIC and conventional method

Component	Conventional method	DIC results
Young's modulus	209.8 *GPa*	199.4 *GPa*
Poisson's ratio	0.282	0.283
Hardening exponent	0.204	0.210

noted that the responses obtained by using a simplified DIC test are in very good agreement with those obtained using conventional procedures. The post necking behaviour of the specimen could not be studied because of paint peel off. In case of fatigue test no peel off was observed as high stress is confined to near crack-tip and thus stretching of paint film is confined to a small region ahead of crack-tip.

ASTM E647 gives Eq. (5) to evaluate stress intensity factor range for ESE(T) specimen for a given load range and crack length.

$$\begin{gathered}\boldsymbol{\alpha = a/W} \\ \boldsymbol{G = 3.97 - 10.88\alpha + 26.25\alpha^2 - 38.9\alpha^3} \\ \boldsymbol{+\,30.15\alpha^4 - 9.27\alpha^5} \\ \boldsymbol{F = \alpha^{\frac{1}{2}}[1.4 + \alpha][1 - \alpha]^{-\frac{3}{2}}G} \\ \boldsymbol{\Delta K = [(P_{max} - P_{min})/(B\sqrt{W})]F}\end{gathered} \tag{5}$$

SIF for a typical case is evaluated. Stress intensity factor for a crack of length 38.2 mm using Eq. (5) and from DIC results is evaluated and compared. Stress intensity factor range evaluated for P_{min} as zero gives stress intensity factor. Stress intensity factor obtained is 49.12 $MPa\sqrt{m}$. ASTM E647-13a also gives elasticity check to ensure the specimen is in elastic region and concepts of LEFM are valid. Eq. (6) gives the elasticity check condition. Specimen is satisfying the check for the given crack length and load.

$$\boldsymbol{(W - a) \geq \left(\frac{4}{\pi}\right)\left(\frac{K_{max}}{\sigma_{YS}}\right)^2} \tag{6}$$

The value of A_{I1} obtained from least squares fitting is 7.6 and the corresponding stress intensity factor is 47.54 $\boldsymbol{MPa\sqrt{m}}$. Plastic zone size is found out by plotting stress variation using Eq. (3) as shown in Fig. 18. Red band in Fig. 18(a) shows the plastic zone boundary and Fig. 18(b) shows the 3D representation of stress near the crack-tip.

5. Summary

Digital image correlation which a popular tool for full-field metrology has been utilized for evaluation of tensile and fracture parameters. Educational and industrial institutes generally procure DIC equipment as a turnkey solution. In present work, DIC has been used with a simplified test set-up. The proposed set-up is used for of tensile and fracture characterization of IS 2062 Gr. E300 steel. Tensile test is carried on a flat specimen and the responses such as Young's modulus, Poisson's ratio and Hardening exponent are estimated from DIC results. To validate the obtained values these tensile parameters are also obtained from strain gauge and extensometer measurements and the results are found to be in close agreement. Stress intensity factor is determined for eccentrically-loaded single edge notch tension (ESE(T)) specimen. The proposed method for evaluation of SIF involves fitting strain field obtained from DIC to strain field equation proposed by Atluri and Kobayashi. The SIF thus obtained is compared with equations of ASTM E647. A good agreement between results obtained from DIC and conventional methods is observed. It can be said that DIC when used with a DSLR as imaging device can be used for carrying experimental studies. It is also observed that as resolution of DSLR camera is generally multi-fold than one supplied with DIC turnkey set-up which makes the proposed set-up suitable for problems with localized deformation like fracture problem.

Acknowledgments

The authors thank the Director and Advisor (Management), CSIR-SERC for their valuable guidance, encouragement and support in the R&D activities. The cooperation and support extended by the technical staff of Fatigue & Fracture Laboratory of CSIR-SERC in carrying out the experimental investigations is gratefully acknowledged.

References

ASTM E1820-18 Standard Test Method for Measurement of Fracture Toughness (2018), *ASTM International*, West Conshohocken, Pennsylvania, U.S.A.

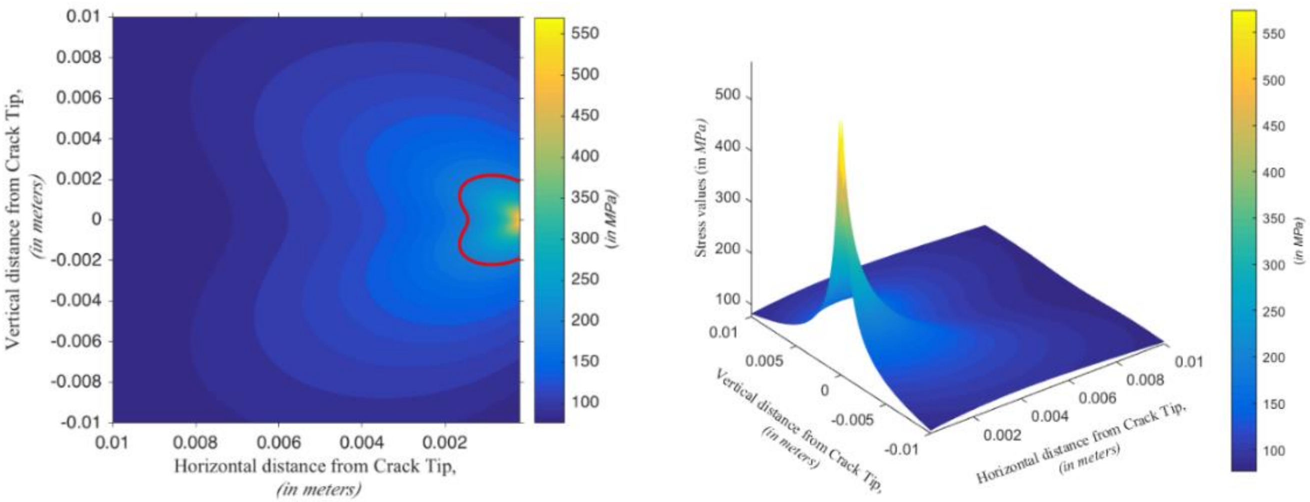

(a) Stress field plot with plastic zone (b) 3D Stress field plot

Fig. 18 Stress field plots

ASTM E647-15e1 Standard Test Method for Measurement of Fatigue Crack Growth Rates (2015), *ASTM International*, West Conshohocken, Pennsylvania, U.S.A.

ASTM E8/E8M-16a Standard Test Methods for Tension Testing of Metallic Materials (2016), *ASTM International*, West Conshohocken, Pennsylvania, U.S.A.

Atluri, S.N. and Kobayashi, A.S. (1993), *Mechanical Responses of Materials*, Handbook of Experimental Mechanics, 1-37.

Ayatollahi, M.R. and Sedighiani, K. (2010), "Crack tip plastic zone under mode I, mode II and mixed mode (I+II) conditions", *Struct. Eng. Mech.*, **36**(5), 575-598.

Bay, B.K., Smith, T.S., Fyhrie, D.P. and Saad, M. (1999), "Digital volume correlation: Three-dimensional strain mapping using X-ray tomography", *Exper. Mech.*, **39**(3), 217-226.

Blaber, J., Adair, B. and Antoniou, A. (2015), "Ncorr: Open-source 2D digital image correlation matlab software", *Exper. Mech.*, **55**(6), 1105-1122.

Buljac, A., Jailin, C., Mendoza, A., Neggers, J., Taillandier-Thomas, T., Bouterf, A., Smaniotto, B., Hild, F. and Roux, S. (2018), "Digital volume Ccrrelation: Review of progress and challenges", *Exper. Mech.*, **58**(5), 661-708.

Dournaux, J.L., Bouvier, S., Aouafi, A. and Vacher, P. (2009), "Full-field measurement technique and its application to the analysis of materials behaviour under plane strain mode", *Mater. Sci. Eng.: A*, **500**(1-2), 47-62.

Grédiac, M., Sur, F. and Blaysat, B. (2016), *The Grid Method for In-Plane Displacement and Strain Measurement: A Review and Analysis*, John Wiley & Sons, Ltd.

Harilal, R., Vyasarayani, C.P. and Ramji, M. (2015), "A linear least squares approach for evaluation of crack tip stress field parameters using DIC", *Opt. Las. Eng.*, **75**, 95-102.

Helm, J.D., Sutton, M.A. and McNeill, S.R. (1996), "Improved three-dimensional image correlation for surface displacement measurement", *Soc. Photo-Opt. Instrument. Eng.*, **35**(7), 1911-1920.

Hild, F., Amine, B., Ludovic, C., Hugo, L., Florent, M., Jan, N., Florent, P., Zvonimir, T. and Stéphane, R. (2016), "Toward 4D mechanical correlation", *Adv. Model. Simulat. Eng. Sci.*, **3**(1), 17.

Jhung, M.J. and Park, Y.W. (1999), "Deterministic structural and fracture mechanics analyses of reactor pressure vessel for pressurized thermal shock", *Struct. Eng. Mech.*, **8**(1), 103-118.

Julien, R. (2007), "From pictures to extended finite elements: Extended digital image correlation (X-DIC) corr'elation d' images num'eriques'etendue (CIN E)", *Sci.*, **335**, 1-8.

Lionello, G. and Luca, C. (2014), "A practical approach to optimizing the preparation of speckle patterns for digital-Image correlation", *Measure. Sci. Technol.*, **25**(10), 107001.

Lu, H., and Cary, P.D. (2000), "Deformation measurements by digital image correlation: Implementation of a second-order displacement gradient", *Exper. Mech.*, **40**(4), 393-400.

Luo, P.F., Chao, Y.J., Sutton, M.A. and Peters, W.H. (1993), "Accurate measurement of three-dimensional deformations in deformable and rigid bodies using computer vision", *Exper. Mech.*, **33**(2), 123-132.

Maire, E. and Withers, P.J. (2014), "Quantitative x-ray tomography", *Int. Mater. Rev.*, **59**(1), 1-43.

Pan, B., Kemao, Q., Huimin, X. and Anand, A. (2009), "Two-dimensional digital image correlation for in-plane displacement and strain measurement: A review", *Measure. Sci. Technol.*, **20**(6), 062001.

Peters, W.H. and Ranson, W.F. (1982), "Digital imaging techniques in experimental stress analysis", *Opt. Eng.*, **21**(3), 427-431.

Rastogi, P.K. (2000), *Photomechanics*, Topics in Applied Physics, Springer Berlin Heidelberg, Berlin, Heidelberg, Germany.

Regez, B., Ying, Z., Tsuchin, C., Jarlen, D. and Ajay, M. (2008), "In-plane bulk material displacement and deformation measurements using digital image correlation of ultrasonic C-scan images", *Struct. Eng. Mech.*, **29**(1), 113-116.

Réthoré, J., Stéphane, R. and François, H. (2007), "From Pictures to Extended Finite Elements: Extended Digital Image Correlation (X-DIC)." *Comptes Rendus - Mecanique* **335**(3), 131-137.

Roux, S. and Hild, F. (2008), "Digital image mechanical identification (DIMI)", *Exper. Mech.*, **48**(4), 495-508.

Shang, S., Yun, G.J., Kunchum, S. and Carletta, J. (2013), "Identification of isotropic and orthotropic constitutive parameters by FEA-free energy-based inverse characterization method", *Struct. Eng. Mech.*, **45**(4), 471-494.

Tippur, H. and Periasamy, C. (2013), *A Digital Gradient Sensor for Nondestructive Evaluation and Stress Analysis*, SPIE Newsroom, March.

Westerweel, J., Elsinga, G.E. and Adrian, R.J. (2013), "Particle image velocimetry for complex and turbulent flows", *Ann. Rev. Flu. Mech.*, **45**(1), 409-436.
Yoneyama, S., Ogawa, T. and Kobayashi, Y. (2007), "Evaluating mixed-mode stress intensity factors from full-field displacement fields obtained by optical methods", *Eng. Fract. Mech.*, **74**(9), 1399-1412.

CC

Nomenclature

a	crack length
K	stress intensity factor
K_{max}	maximum stress intensity factor
ΔK	applied stress intensity range
$\{r, \varphi\}$	polar coordinates
σ_x, σ_y, τ_{xy}	stress components in plane stress
v	Poisson's ratio
W	width of specimen
B	breadth of specimen
σ_{YS}	yield stress